


## Universal features of the stick-slip dynamics of an intruder moving through a confined granular medium

Luis A. Pugaloni <sup>1,\*</sup>, C. Manuel Carlevaro <sup>2</sup>, Ryan Kozłowski <sup>3</sup>, Hu Zheng <sup>4</sup>,

Lou Kondic <sup>5</sup> and Joshua E. S. Socolar <sup>6</sup>

<sup>1</sup>*Departamento de Física, Facultad de Ciencias Exactas y Naturales, Universidad Nacional de La Pampa, CONICET, Uruguay 151, 6300 Santa Rosa (La Pampa), Argentina*

<sup>2</sup>*Instituto de Física de Líquidos y Sistemas Biológicos, CONICET, 59 789, 1900 La Plata, Argentina*  
and *Departamento de Ingeniería Mecánica, Universidad Tecnológica Nacional, Facultad Regional La Plata, Avenida 60 Esquina 124, 1900 La Plata, Argentina*

<sup>3</sup>*Physics Department, Berea College, Berea, Kentucky 40404, USA*

<sup>4</sup>*Department of Geotechnical Engineering, College of Civil Engineering, Tongji University, Shanghai 200092, China*

<sup>5</sup>*Department of Mathematical Sciences and Center for Applied Mathematics and Statistics, New Jersey Institute of Technology, Newark, New Jersey 07102, USA*

<sup>6</sup>*Department of Physics, Duke University, Durham, North Carolina 27708, USA*



(Received 14 December 2021; accepted 11 March 2022; published 21 April 2022)

Experiments and simulations of an intruder dragged by a spring through a two-dimensional annulus of granular material exhibit robust force fluctuations. At low packing fractions ( $\phi < \phi_0$ ), the intruder clears an open channel. Above  $\phi_0$ , stick-slip dynamics develop, with an average energy release that is independent of the particle-particle and particle-base friction coefficients but does depend on the width  $W$  of the annulus and the diameter  $D$  of the intruder. A simple model predicts the dependence of  $\phi_0$  on  $W$  and  $D$ , allowing for a data collapse for the average energy release as a function of  $\phi/\phi_0$ . These results pose challenges for theories of mechanical failure in amorphous materials.

DOI: [10.1103/PhysRevE.105.L042902](https://doi.org/10.1103/PhysRevE.105.L042902)

The reaction force associated with the deformation of a sample subjected to an intruding object is a fundamental characteristic of the material. The mechanical properties of granular materials, such as soils, are routinely probed by penetration tests employing intruders that are large compared to the grains [1]. Interest in the micromechanics of granular materials has also prompted studies of the response of photoelastic granular materials to loads applied at the grain scale [2–6]. In recent decades there has been interest in the dynamical response of granular materials to intruding objects that are dragged through the bulk of the sample [7–13]. In most cases the intruders are much larger than the grains that form the relevant part of the material, but there is also growing interest in the response to a grain-sized intruder, as such a setup provides insight into the micromechanics of granular media rather than bulk properties [14].

In this Letter we report results from experiments and simulations on the stick-slip dynamics of a grain-size intruder driven through a circular annulus with fixed boundaries filled with photoelastic disks. We find that the energy dissipation associated with slip events is insensitive to the details of the particle-particle interactions and depends in a surprisingly simple manner on the packing fraction  $\phi$ , the system size  $W$ , and the intruder size  $D$ . The granular sample is confined at constant volume and we drive the intruder in the azimuthal

direction at a fixed radius. We find a critical packing fraction  $\phi_0$  (which increases for increasing width  $W$  and decreasing intruder size  $D$ ) below which the intruder clears an open channel in the material and moves freely after a few revolutions. Moreover, we show that data for the average amount of energy dissipated in a slip event collapse when plotted against the rescaled parameter  $\phi/\phi_0 - 1$ . Using a simple model, we predict that  $\phi_0 = \phi_{\max}(W - D - 2kd)/W$ , where  $d$  is the typical grain size,  $\phi_{\max}$  is the maximum bulk packing fraction, and  $k$  is a phenomenological  $O(1)$  parameter that characterizes the width of the lower density boundary layers bordering the open channel. We note that the dependence on  $W$  suggests that in this system the stick-slip dynamics is a finite-size effect. As  $W$  increases, the range of packing fractions supporting stick-slip dynamics shrinks, presumably approaching zero in the infinite system limit.

*The system.* The granular system considered in this paper consists of a bidisperse mixture of disks forming a quasi-two-dimensional (2D) monolayer through which an intruding particle is pulled (see sketch in Fig. 1). The diameter ratio between small ( $d_s$ ) and large ( $d_l$ ) disks is  $\approx d_l/d_s \approx 1.25$  and the number ratio of small to large disks approximately is 1.1:1. (A 2.75:1 ratio was also tested for a few sets). We note that the response of a granular sample is strongly dependent on the boundary conditions imposed (constant pressure versus constant volume) and the forcing protocol (constant force versus constant velocity) [14,16–19]. In the present case, the medium is confined to a fixed-volume annular area of inner

\*luis.pugaloni@exactas.unlpam.edu.ar

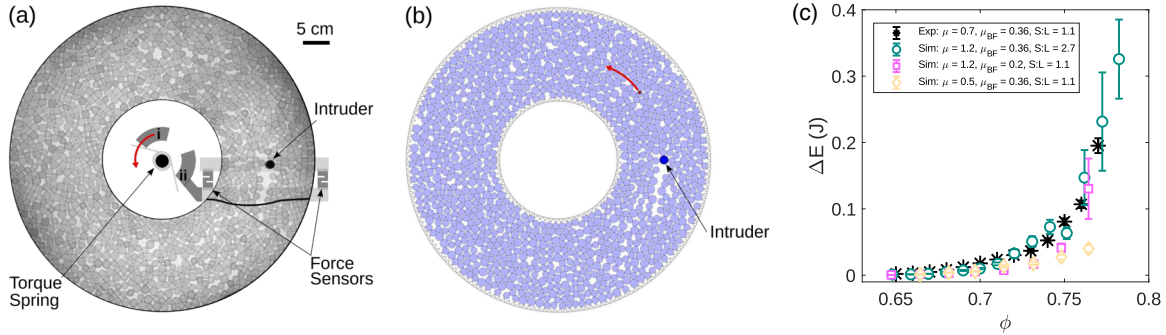


FIG. 1. (a) Schematic of the experimental setup. The end (i) of the torque spring is driven at a constant angular velocity while the end (ii) is fixed to the arm that holds the intruder. The 2D granular medium is composed of a layer of bidisperse polyurethane disks. (b) Sample snapshot of a simulation. The dot indicates the driven end of the torque spring. The other end of the spring is attached to the intruder (dark blue particle). The static inner and outer boundaries are formed by equilateral triangles. Reproduced with permission from Ref. [15]. (c) Mean energy drop at the slips  $\langle \Delta E \rangle$  as a function of  $\phi$  for different mix ratios, basal friction coefficients, and particle-particle friction coefficients (experiments and simulations). Error bars correspond to the standard error of the mean. As a reference, the elastic energy of the torque spring when compressed by the angle subtended by ten small-particle radii at the radial position of the intruder is 0.09 J.

radius  $R_{in}$ , radial width  $W$ , and outer radius  $R_{in} + W$ . The intruding particle, with diameter  $D$ , is pushed by a torque spring at a fixed radius  $R_{in} + W/2$ . The end of the spring not attached to the intruder is rotated at a low, fixed rate to slowly apply stress on the granular medium via the localized intruding grain. At high packing fractions stick-slip dynamics are observed. When in the stick-slip regime, the medium exhibits *sticking periods* of quasistatic particle configurations and increasing stress interspersed with rapid stress-relieving *slip events* in which the medium plastically deforms and the intruder slides in the azimuthal direction until a stable configuration of grains stops it, initiating a new sticking period. In all cases, the driving rate is sufficiently slow that decreasing it further causes no observable change in the stick-slip dynamics.

As the intruder penetrates the system, significant heterogeneities form in the local packing fraction. Most importantly, the intruder leaves an open area (wake) behind it as grains are densely packed into the annular areas outside of the intruder’s path. As the global packing fraction decreases, the extent of the wake behind the intruder grows on average until, at a low enough *global* packing fraction, it becomes an open channel that extends all the way around the annulus so that the intruder no longer interacts with any grains. To understand the dynamics of the intruder as the channel length approaches the entire length of the intruder’s path, we vary  $\phi$  and  $D$  (both in experiments and simulations) and  $W$  (in simulations only). Details of the experiments and simulation methods can be found in previous papers [15,20]. Here we provide only a brief description.

In experiments, the intruding particle is suspended from a cantilever into the quasi-two-dimensional annular channel of disks. A stepper motor rotates one end of a torque spring (stiffness  $\kappa_0 = 0.38$  Nm/rad) at a fixed rate ( $\omega_0 = 0.12$  rad/s) and the cantilever is attached to the other end of the spring. The bidisperse polyurethane disks have interparticle friction  $\mu = 0.7 \pm 0.1$  and basal friction  $\mu_{BF} = 0.25 \pm 0.05$  and are of sizes  $d_s = 1.280 \pm 0.001$  cm and  $d_l = 1.601 \pm 0.002$  cm. The inner radius of the channel is  $R_{in} \approx 8.4d_s$ , and the width is  $W \approx 14d_s$ . Load cells measure the total force that the

grains exert on the intruder, and the dynamics of the intruder is monitored via video tracking. Experiments are done with various packing fractions for each of six intruder sizes  $D = [5.2, 3.7, 3.0, 2.0, 1.5, 1.0]d_s$ .

In simulations, we model this system using Box2D, a contact dynamics discrete element approach developed for handling perfectly rigid bodies of arbitrary shape [21]. The parameters in this system, such as friction coefficients and size ratios, are consistent with those of the experiments; excellent agreement has been found between experiments and simulations of this system in previous work [15]. In the simulations,  $\phi$ , basal friction, intergrain friction, small to large grain ratio, pulling spring constant,  $D$ , and  $W$  are varied.

**Results.** To characterize the stick-slip steady state dynamics, we have measured the drop,  $\Delta E$ , of the spring potential energy at each slip event, determining its mean and standard error. A sample time series of the force sensor, distributions of  $\Delta E$  showing that its mean value is a meaningful statistical descriptor, and data for additional measures, such as force drop and duration of sticking periods, are presented in the Supplemental Material [22].

Figure 1(c) shows the average energy drop,  $\langle \Delta E \rangle$ , over the set of detected slip events as a function of  $\phi$  for a set of experiments and simulations with  $D = 1.26d_s$  and different small to large grain ratios, particle-base friction coefficients, and interparticle friction coefficients. Below  $\phi_0 \approx 0.64$  the stick-slip dynamics is no longer observed due to the formation, after a few revolutions of the intruder, of an open channel in the granular medium that allows the intruder to move without contacting any particles. When  $\phi$  approaches the jamming value of  $\approx 0.8$ , there is an apparent divergence in the mean energy drop in a slip event. Other works, see in particular Ref. [23], have focused on this divergence in similar systems. Here we turn our attention to the onset of stick-slip behavior, which occurs at  $\phi_0$ .

The transition at  $\phi_0$  has not been reported in other studies on intruders mainly because most of these studies are carried out in a 3D system under gravity [13,18]. Under such conditions, the intruder’s wake is constantly filled in. In cases where constant volume conditions in 2D were used and a

wake developed, the focus was on packing fractions close to the jamming point rather than packing fractions at very low reaction forces [8,17,23], and often a steady state was never achieved. According to previous experiments, the extent of the wake becomes a sensitive parameter to identify different aspects of the dynamics (i.e., stick-slip versus full jamming) [23]. In a previous work [19] utilizing a similar Couette geometry, the granular sample was continuously stirred behind the intruder to remove its wake. For this stirred system, a crossover in the mean force as a function of  $\phi$  (from linear to power law with exponent 1.53) was observed at a packing fraction  $\phi_0$  similar to what we observe in our experiments [19]. For our nonstirred system this becomes a clearly identifiable transition.

As mentioned above, stick-slip dynamics develop for  $\phi > \phi_0$ , and  $\langle \Delta E \rangle$  can be measured, increasing continuously with  $\phi$  up to  $\phi_c \approx 0.8$ , where the system completely jams [see Fig. 1(c)]. Beyond  $\phi_c$ , the spring force increases until particles in experiments buckle out of plane, or, in simulations, numerical instabilities develop or the maximum run time is reached.

A remarkable feature in Fig. 1(c) is the collapse of the data obtained from the different interaction parameters and the grain number ratios. Note that no scaling has been applied to either the  $\langle \Delta E \rangle$  or the  $\phi$  axes. This universal response resembles the well-known behavior of sheared granular materials in the limit of low inertial number  $I$  [24]. In this limit, the effective friction  $\mu(I)$  and the shear strength are insensitive to details of the grain-grain interactions [25] and the particle size distribution [26]. In our intruder scenario, however, the stick-slip behavior differs significantly from the dynamics observed in a simple shear experiment.

It is important to mention that  $\Delta E$  is independent of basal friction for  $\mu_{\text{BF}} > 0.2$ . For very low basal friction, particles set in motion behind the intruder after a slip tend to remain in motion, filling in the wake left by the intruder before coming to rest. This effect resembles the stirring mechanism implemented in Ref. [19]. This leads to a different dynamics over all, which we do not investigate further in the present work.

We explore now the effect of geometric factors, including intruder and system size, on the intruder dynamics, which have been shown to affect the force fluctuations [23]. In Fig. 2(a) we show  $\langle \Delta E \rangle$  obtained from simulations as a function of  $W$  with fixed  $\phi$  ( $\phi = 0.68$ ). A change in  $W$  implies a change in the radial position  $R$  of the intruder; the same torque spring and angular drive velocity would then lead to a different tangential stiffness and tangential velocity. To keep the effective linear stiffness of the spring and the effective tangential driving speed the same in all cases, we set the spring constant  $\kappa = \kappa_0(R/R_0)^2$  and the angular velocity of the driver  $\omega = \omega_0(R_0/R)$ , where  $R_0$  is the radial position for our experimental system size that we use as reference. We find that  $\langle \Delta E \rangle$  decreases with increasing  $W$ , suggesting that stick-slip is a finite-size effect and may disappear for large system sizes. Similarly, in Fig. 2(b) we plot  $\langle \Delta E \rangle$  as a function of the intruder diameter  $D$  at  $\phi = 0.68$ . Here  $\langle \Delta E \rangle$  is zero for very small intruders, becomes finite at a minimum intruder size, and then increases smoothly with  $D$  in agreement with Refs. [19,23].

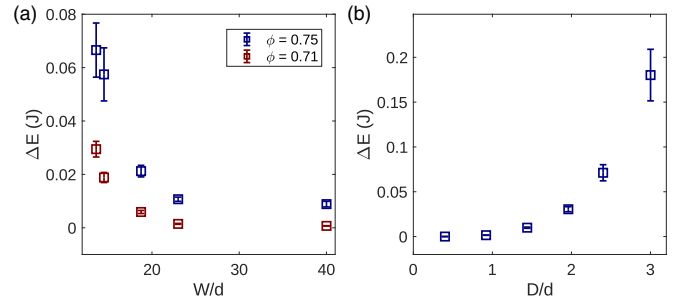


FIG. 2.  $\langle \Delta E \rangle$  as a function of (a) the channel width  $W$  (at  $\phi = 0.75$  and  $D = 1.26d_s$ ) and (b) the intruder size  $D$  (at  $\phi = 0.68$  and  $W = 14d_s$ ). Here,  $d_s$  is the diameter of the small particles. In panel (a) we adjust  $\kappa$  and the drive angular velocity so that the spring is pulled at the same tangential speed, fixing the linear rate of force increase when the intruder is stationary. Error bars correspond to the standard error of the mean.

The data collapse shown in Fig. 1(c) suggests that we plot  $\langle \Delta E \rangle$  as a function of  $\phi$  for different values of  $D$  and  $W$ . Figure 3(a) shows experimental data for seven choices of  $D$ . We note that the transition to zero force (when the open channel forms) occurs at a different value  $\phi_0$  for each  $D$ . The data collapse onto a single curve when plotted against  $\phi/\phi_0 - 1$ , a measure of the relative distance to the transition, as shown in Fig. 3(b). The value of  $\phi_0$  for each  $D$  was estimated by lowering the packing fraction  $\phi$  until no steady-state dynamics were observed. Surprisingly, there is no need for any rescaling of the energies; furthermore, the data shown in Fig. 1(c) [see black symbols in Fig. 3(b)] also lie on the same curve.

The full data collapse we observe can be explained by a simple argument for the dependence of  $\phi_0$  on  $W$  and  $D$ . We assume that  $\phi_0$  corresponds to the highest  $\phi$  (global packing fraction) at which the intruder is able to clear a channel that will allow it to move freely without contacting particles after a few revolutions. Therefore,  $\phi_0$  can be computed from the area of the Couette cell  $A_{\text{Couette}} = \pi(R_{\text{out}}^2 - R_{\text{in}}^2)$ , the area  $A_{\text{free}} = \pi[(R_{\text{in}} + W/2 + D/2)^2 - (R_{\text{in}} + W/2 - D/2)^2]$  of the free channel necessary for the intruder to move freely, and the maximal packing fraction  $\phi_{\text{max}}$  at which particles are packed into the two regions on each side of the intruder's path around

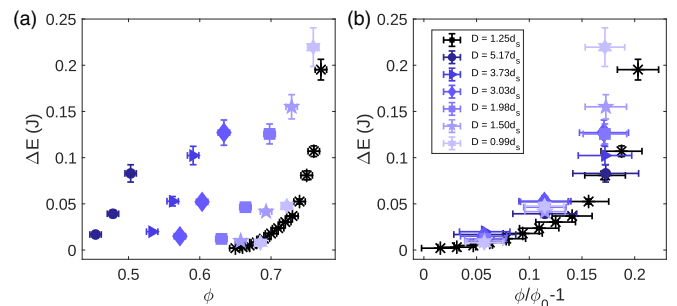


FIG. 3. (a)  $\langle \Delta E \rangle$  as a function of  $\phi$  for different intruder sizes. (b) Same as panel (a) as a function of the rescaled parameter  $\phi/\phi_0 - 1$ . The black symbols correspond to the experimental data from Fig. 1(c).

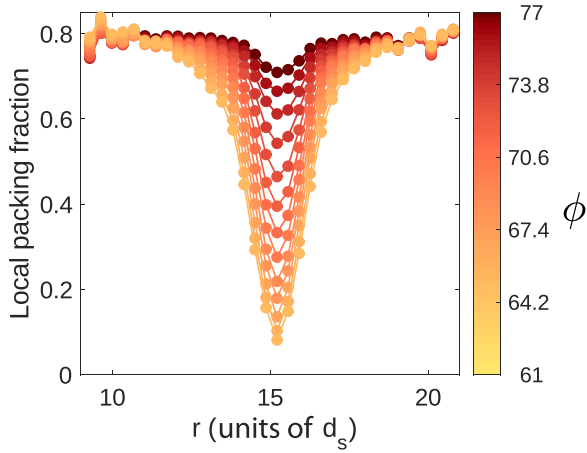


FIG. 4. Local packing fraction extracted from experiments with  $D = 1.26d_s$  as a function of distance from the center of the Couette  $r$  and for different global packing fractions  $\phi$  (see color scale), averaged over all steady-state sticking periods.

the center of the annulus. We have

$$\phi_0 = \frac{\phi_{\max}(A_{\text{Couette}} - A_{\text{free}})}{A_{\text{Couette}}} = \phi_{\max} \frac{W - D}{W}. \quad (1)$$

We have measured  $\phi_{\max}$  in the experiments from average local  $\phi$  profiles shown in Fig. 4, and the value is  $\phi_{\max} \approx 0.79$  at the boundaries. The local packing fraction as a function of radial position in the channel is computed using a sliding annular window of width  $\sim 1.4d_s$ . For a given annular window, the area occupied by particles is divided by the window's area for each sticking period configuration, and these results are then averaged. As expected, these local packing fraction profiles are not simple square wells; a clear boundary layer appears at each side of the intruder. To account for the boundary layer (which we assume to be roughly constant in width), we introduce a correction to Eq. (1) following a strategy similar to previous works [27,28]. The corrected equation is

$$\phi_0 = \phi_{\max} \frac{W - D - 2kd}{W}, \quad (2)$$

where  $k$  is a phenomenological parameter that measures the width of each of the two boundary layers in units of grain diameters. Figure 5 shows the values of  $\phi_0$  estimated from Fig. 3 as a function of  $W^* = (W - D - 2kd)/W$ . Having obtained the value  $k$  from experiments carried out using different intruder sizes  $D$ , we use Eq. (2) to compute  $\phi_0$  for all other cases of  $W$  and  $D$  considered in this work. As is demonstrated below, statistical properties of the intruder's dynamics indeed collapse when plotted against  $\phi/\phi_0 - 1$  with  $\phi_0$  computed in this manner.

Figure 6 shows  $\langle \Delta E \rangle$  for simulations carried out with different  $D$  and  $W$  at fixed packing fractions. Figure 6(b) shows the data when plotted against  $\phi/\phi_0 - 1$ . The collapse suggests that one single parameter ( $\phi_0$ ) suffices to describe the stick-slip response of the granular system constrained at constant volume when an intruder attached to a spring is dragged at low speed. Again, these data also collapse with the data from the experiments and simulations shown in Figs. 1(c) and 3 (see black symbols).

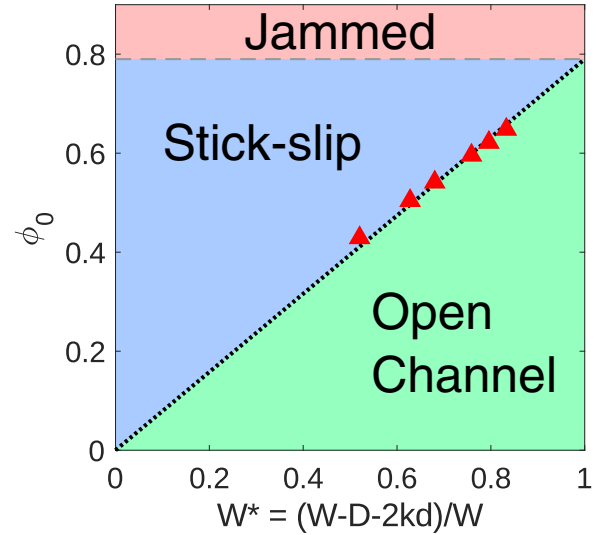


FIG. 5.  $\phi_0$  as a function of  $(W - D - 2kd)/W$ , with  $k = 0.62$ , obtained by linear regression. The black dotted line corresponds to Eq. (2) with  $\phi_{\max} = 0.79$ , and the horizontal gray dashed line corresponds to  $\phi_{\max}$ .

Figure 5 suggests a nontrivial prediction regarding the limit of infinitely large systems. If  $W \gg D$ , then  $W^* \rightarrow 1$ . In this limit, the value of  $\phi_0$  tends to 0.79. This means that no force will be exerted on the intruder for  $\phi < 0.79$ . As we mentioned above, when  $\phi \gtrsim 0.8$  we observe a complete jamming of the system. Therefore, the actual range of packing fractions for which a stick-slip steady state can be established becomes very narrow for large systems, possibly vanishing in the large  $W$  limit. Of course, the  $W^* \rightarrow 1$  limit has to be taken with caution. The time taken to complete a revolution and eventually reach the steady state diverges with the system size in this annular geometry.

**Conclusions.** We have described a dynamical transition observed when an intruder is dragged through a granular system confined by a container with fixed volume. In our experiments and simulations, the granular material reaches a steady state after the intruder passes through a few revolutions. Due to the friction with the substrate, particles pushed aside tend to rest outside of the intruder's path in

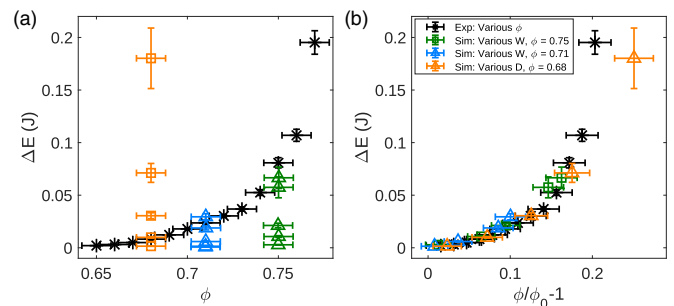


FIG. 6. (a)  $\langle \Delta E \rangle$  as a function of  $\phi$  for a range of configurations of the system that we tested with various  $D$  and  $W$ . (b)  $\langle \Delta E \rangle$  as a function of  $\phi/\phi_0 - 1$  for the data in panel (a). The actual value of  $\phi_0$  in each case has been estimated by using Eq. (2). The black symbols correspond to the experimental data from Fig. 1(c).



subsequent passes. At low packing fractions, the intruder is thus able to open a channel so that in the steady state no resistance is supplied by the medium. Above a critical packing fraction  $\phi_0$ , a sharp transition occurs and the channel cannot be fully opened, which leads to a finite mean reaction force that increases with the global packing fraction  $\phi$ .

We have found that  $\phi_0$  and  $\langle \Delta E \rangle(\phi)$  are universal in the sense that over a broad parameter range they are independent of the details of the particle-particle interaction, the particle-substrate interaction, and the particle size distribution. While they are very sensitive to the system size and the intruder size,  $\langle \Delta E \rangle(\phi)$  can be collapsed onto a single master curve if plotted against  $\phi/\phi_0 - 1$ . We have proposed a simple model for the dependence of  $\phi_0$  on  $W$  and  $D$  that is in excellent agreement with the data. While we have studied this model with one particular driving spring constant, the collapse of statistics related to stick-slip is pictured to be robust, even though the time and energy scales of stick-slip will change when the driving spring changes. Future works may explore whether the collapse we explain is robust in other contexts,

for example, when the spring is infinitely stiff and the intruder is driven at a constant velocity. Further work is also needed in the direction of analysis of force networks, in particular in light of friction independence of our results for the energy drop (for sufficiently large friction). Some preliminary work in this direction can be found in Refs. [29,30]. We lastly note that our results may have implications for 3D systems, as demonstrated in recent experiments [31] where the drag force on a submerged intruder reaches a steady state after the intruder retraces its path in a 3D granular material. Our findings may also find particular utility in the context of testing various novel theoretical approaches for dense granular media such as nonlocal rheology models [32,33].

This work was supported by the U.S. Army Research Office through Grant No. W911NF-18-1-0184 and by the Keck Foundation. R.K. thanks the Department of Physics, Duke University, where the experimental work was conducted. M.C. is thankful for the financial support from CONICET (Grant No. PUE 2018 229 20180100010 CO) and UTN (Grant No. MAUTILP0007746TC).

- 
- [1] G. Sanglerat, *The Penetrometer and Soil Exploration* (Elsevier, Amsterdam, 2012).
  - [2] J. Geng, D. Howell, E. Longhi, R. P. Behringer, G. Reydellet, L. Vanel, E. Clément, and S. Luding, *Phys. Rev. Lett.* **87**, 035506 (2001).
  - [3] J. Geng and R. P. Behringer, *Phys. Rev. Lett.* **93**, 238002 (2004).
  - [4] I. Goldhirsch and C. Goldenberg, *Eur. Phys. J. E* **9**, 245 (2002).
  - [5] A. P. F. Atman, P. Brunet, J. Geng, G. Reydellet, G. Combe, P. Claudin, R. P. Behringer, and E. Clément, *J. Phys.: Condens. Matter* **17**, S2391 (2005).
  - [6] B. P. Tighe and J. E. S. Socolar, *Phys. Rev. E* **77**, 031303 (2008).
  - [7] A. Seguin, C. Coulais, F. Martinez, Y. Bertho, and P. Gondret, *Phys. Rev. E* **93**, 012904 (2016).
  - [8] R. Candelier and O. Dauchot, *Phys. Rev. Lett.* **103**, 128001 (2009).
  - [9] A. Fiege, M. Grob, and A. Zippelius, *Granular Matter* **14**, 247 (2012).
  - [10] T. Faug, *Eur. Phys. J. E* **38**, 34 (2015).
  - [11] S. Kumar, K. A. Reddy, S. Takada, and H. Hayakawa, [arXiv:1712.09057](https://arxiv.org/abs/1712.09057).
  - [12] S. Takada and H. Hayakawa, *Granular Matter* **22**, 6 (2020).
  - [13] J. E. Hilton and A. Tordesillas, *Phys. Rev. E* **88**, 062203 (2013).
  - [14] A. Tordesillas, J. E. Hilton, and S. T. Tobin, *Phys. Rev. E* **89**, 042207 (2014).
  - [15] C. M. Carlevaro, R. Kozłowski, L. A. Pugnaloni, H. Zheng, J. E. S. Socolar, and L. Kondic, *Phys. Rev. E* **101**, 012909 (2020).
  - [16] R. Candelier and O. Dauchot, *Phys. Rev. E* **81**, 011304 (2010).
  - [17] C. J. Olson Reichhardt and C. Reichhardt, *Phys. Rev. E* **82**, 051306 (2010).
  - [18] I. Albert, P. Tegzes, R. Albert, J. G. Sample, A. L. Barabási, T. Vicsek, B. Kahng, and P. Schiffer, *Phys. Rev. E* **64**, 031307 (2001).
  - [19] J. Geng and R. P. Behringer, *Phys. Rev. E* **71**, 011302 (2005).
  - [20] R. Kozłowski, C. M. Carlevaro, K. E. Daniels, L. Kondic, L. A. Pugnaloni, J. E. S. Socolar, H. Zheng, and R. P. Behringer, *Phys. Rev. E* **100**, 032905 (2019).
  - [21] E. Catto, Iterative dynamics with temporal coherence, Technical report, Crystal Dynamics, Menlo Park, California (2005), Available at [https://box2d.org/files/ErinCatto\\_IterativeDynamics\\_GDC2005.pdf](https://box2d.org/files/ErinCatto_IterativeDynamics_GDC2005.pdf).
  - [22] See Supplemental Material at <http://link.aps.org/supplemental/10.1103/PhysRevE.105.L042902> for sample signals from the force sensor and additional plots showing the collapse of other stick-slip dynamic descriptors plotted against  $\phi/\phi_0 - 1$ .
  - [23] E. Kolb, P. Cixous, N. Gaudouen, and T. Darnige, *Phys. Rev. E* **87**, 032207 (2013).
  - [24] G. MiDi, *Eur. Phys. J. E* **14**, 341 (2004).
  - [25] F. da Cruz, S. Emam, M. Prochnow, J.-N. Roux, and F. Chevoir, *Phys. Rev. E* **72**, 021309 (2005).
  - [26] D. Cantor, E. Azéma, P. Sornay, and F. Radjai, *Phys. Rev. E* **98**, 052910 (2018).
  - [27] K. W. Desmond and E. R. Weeks, *Phys. Rev. E* **80**, 051305 (2009).
  - [28] W. A. Beverloo, H. A. Leniger, and J. Van de Velde, *Chem. Eng. Sci.* **15**, 260 (1961).
  - [29] R. Kozłowski, H. Zheng, K. E. Daniels, and J. E. S. Socolar, *EPJ Web Conf.* **249**, 06010 (2021).
  - [30] R. Kozłowski, H. Zheng, K. E. Daniels, and J. E. S. Socolar, *Soft Matter* **17**, 10120 (2021).
  - [31] F. Guillard, Y. Forterre, and O. Pouliquen, *Phys. Rev. Lett.* **110**, 138303 (2013).
  - [32] O. Pouliquen and Y. Forterre, *Philos. Trans. Royal Soc., A* **367**, 5091 (2009).
  - [33] K. Kamrin and G. Koval, *Phys. Rev. Lett.* **108**, 178301 (2012).